J. Plasma Physics (1999), *vol.* 61, *part* 3, *pp.* 425–433. Printed in the United Kingdom
© 1999 Cambridge University Press

Three-dimensional electromagnetic relativistic particle-in-cell code VLPL (Virtual Laser Plasma Lab)

A. PUKHOV

Max-Planck-Institut für Quantenoptik, D-85748 Garching, Germany

(Received 4 June 1998 and in revised form 14 October 1998)

The three-dimensional particle-in-cell (PIC) code VLPL (Virtual Laser Plasma Lab) allows, for the first time, direct fully electromagnetic simulations of relativistic laser–plasma interactions. Physical results on relativistic self-focusing in underdense plasma are presented. It is shown that background plasma electrons are accelerated to multi-MeV energies and 10^4 T magnetic fields are generated in the process of self-focusing at high laser intensities. This physics is crucial for the fast ignitor concept in inertial confinement fusion. Advances in the numerical PIC algorithm used in the code VLPL are reviewed here.

1. Introduction

We are currently seeing an almost-explosive progress in short-pulse laser technology, which has resulted in a dramatic increase in achieved laser powers and intensities (Mourou et al. 1998). When such multi-terawatt or even petawatt (Key et al. 1998) laser pulses at intensities of 10^{18}–10^{21} W cm^{-2} interact with plasmas, a wide spectrum of interesting nonlinear effects occurs. Background plasma electrons are accelerated to multi-MeV energies (Modena et al. 1995; Umstadter et al. 1996; Key et al. 1998), forming 100 kA currents (Pukhov and Meyer-ter-Vehn 1996, 1997) and generating 10^4 T magnetic fields (Pukhov and Meyer-ter-Vehn 1996; Askar'yan et al. 1994). The change in the plasma refractive index due to these relativistic electrons concomitant with the laser pulse contributes to the pulse self-guiding and leads to the filament coalescence (Pukhov and Meyer-ter-Vehn 1996; Borghesi et al. 1997). The underlying physics is essentially kinetic and strongly nonlinear, thus precluding the use of hydrodynamic plasma models and/or a paraxial/quasistatic description of the laser pulse (Esarey et al. 1996). In this situation, one is forced to use a fully kinetic description of the plasma.

The most powerful tools for these simulations are relativistic fully electromagnetic particle-in-cell (PIC) codes (Birdsall and Langdon 1991). The PIC codes are based on fundamental equations for the particle and field dynamics, and provide the most detailed kinetic description of plasmas. Fortunately, the super-intense laser pulses are extremely short, 100 fs–1 ps, i.e. only tens to hundreds of laser periods for a 1 μm radiation wavelength. It is this short pulse duration that makes direct PIC simulations of relativistic laser–plasma interactions feasible.

https://doi.org/10.1017/S0022377899007515 Published online by Cambridge University Press

Considering a PIC simulation, one can speak about a numerical or 'virtual' plasma experiment. Such virtual plasma experiments are of a great value for understanding what is going on in real experiments. Two-dimensional (2D) PIC simulations have already become a 'workhorse' in studies of relativistic laser–plasma interactions (Dawson 1995), and the first three-dimensional (3D) PIC simulations of actual experiments with the code VLPL (Virtual Laser Plasma Lab) have been reported recently (Borghesi et al. 1997; Pukhov and Meyer-ter-Vehn 1998).

In this paper, we present results of 3D PIC simulations of relativistic self-focusing in underdense plasmas and describe the new features of the code VLPL that made it possible for the first time to simulate actual laser–plasma experiments in 3D. The code VLPL is a fully electromagnetic explicit PIC code. It exists in 2D and 3D geometries and runs on the Cray T3E-600 LC688 with 688 application processor elements (PEs), 3.3 ns clock time each, and 85 gigabyte overall memory at Rechenzentrum Garching.

VLPL allows for direct 3D simulations of actual laser–plasma experiments due to:

(i) improvements in the numerical scheme which gives high-quality results even on coarse meshes with large time steps;

(ii) the use of massively parallel processing with more than 90% parallel efficiency and linear performance scaling with the number of processors;

(iii) aggressive single-processor optimization of the code: the new object-oriented C++ version of VLPL runs at more than 100 MFLOP per processor on the Cray T3E-600.

2. Self-focusing in underdense plasmas

A laser beam propagating in an underdense plasma with a plasma frequency ω_p smaller than the laser frequency ω undergoes relativistic self-focusing as soon as its total power P exceeds the critical value (Borisov et al. 1992)

$$P_c \approx 17 \left(\frac{\omega}{\omega_p}\right)^2 \text{ GW}. \tag{2.1}$$

The self-focusing is due to the relativistic mass increase of plasma electrons and the ponderomotive expulsion of electrons from the pulse region. Both effects lead to a local decrease in the plasma frequency and an increase in the refractive index. The medium then acts as a positive lens.

2.1. Laser power close to critical: multi-MeV electrons

Self-focusing of a laser with $P > P_c$ in 3D geometry leads to strong intensity enhancement at the axis. Simultaneously, a 3D self-modulation of the laser pulse sets in (Esarey et al. 1994), generating large-amplitude plasma waves. These waves break owing to 1D (Akhieser and Polovin 1956; Bulanov et al. 1995) or 2D (Bulanov et al. 1997) mechanisms producing fast electrons; these can be trapped and accelerated to high energies, as has been observed recently in experiments (Umstadter et al. 1996; Wagner et al. 1997). Detailed studies show that these fast electrons appear only above some threshold in the laser power (Wagner et al. 1997) and plasma density (Fedoseevs et al. 1997); this threshold is about $P \approx P_c$.

https://doi.org/10.1017/S0022377899007515 Published online by Cambridge University Press

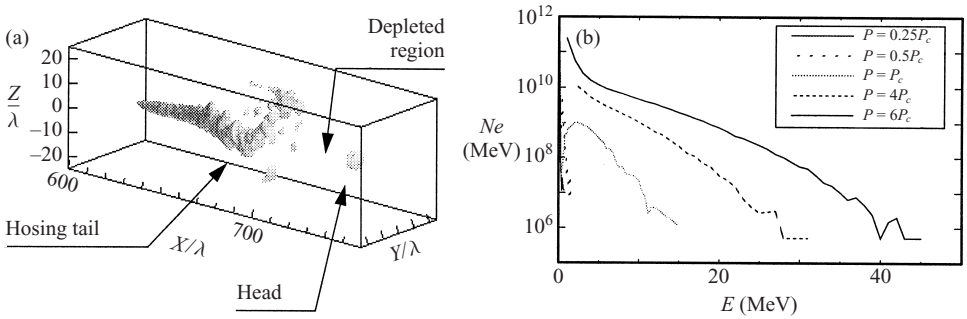


Figure 1. (a) Energy spectra of electrons accelerated in a plasma with density $n = 0.036n_c$ for different laser powers. (b) Laser pulse with initial $P = 4P_c$, after passing 0.6 mm distance.

We have carried out a series of 3D PIC simulations of a Gaussion laser pulse with radius $r = 8.5$ μm (at $1/e^2$ from the maximum intensity), and duration 460 fs propagating through a plasma with density $n = 0.036n_c$ over a 0.6 mm distance. The laser was focused at the entrance into the plasma. The laser power was varied from 0.1 P_c to 10 P_c, where $P_c = 470$ GW under these conditions. The energy spectra of accelerated electrons are shown in Fig. 1(a).

The energetic electrons appear at $P > P_c$. Surprisingly, *no sharp cutoff* associated with the dephasing limit is observed in the energy spectrum. Instead, the energy distribution rather resembles a Boltzman one, with a long smooth roll-out at high energies. The 'effective temperature' of the distribution increases with laser power.

The characteristic evolution of laser pulse with $P = 4P_c$ is shown in Fig. 1(b). The pulse has split into its low-power head, diffracting in the plasma, a depleted region behind it, where the laser energy has been spent producing the plasma wake, and the focused and modulated tail of the pulse, which experences hosing (Shvets and Wurtele 1994).

2.2. High laser power: magnetic fields and filamentation

When a laser pulse with power far above the threshold (2.1) propagates through a slightly underdense plasma, it is subject to the relativistic filamentation instability, which can prevent energy accumulation in a single channel. However, at intensities far above I_{18}, i.e. when $a > 1$, a new important effect appears. The laser pulse drives strong currents of relativistic electrons in the direction of light propagation, magnetizing the plasma (Pukhov and Meyer-ter-Vehn 1996; Bulanov et al. 1995). The generated quasistatic magnetic field is $B^s_\perp = (en_e)2\pi r$ at a distance r from the beam axis. The field $B^s_\perp$ may become as strong as the magnetic field of the light wave itself, which is $B = aB_0$ in units of $B_0 = m\omega/e$. For light of wavelength $\lambda = 2\pi c/\omega = 1$ μm, one obtains $B_0 \approx 10^4$ T. In units of B_0, the quasistatic magnetic field is

$$\frac{B^s_\perp}{B_0} = \frac{n_e}{n_c}\frac{\pi r}{\lambda}. \tag{2.2}$$

The magnetic field *pinches the concomitant relativistic electrons*, changing the plasma refraction. This leads to nonlocal interaction between light filaments, their mutual attraction, and final coalescence into a single 'Super-Channel'.

3D PIC simulations (see Fig. 2) reveal this effect (Pukhov and Meyer-ter-Vehn 1996). The laser pulse sequentially passes through an unstable filamentory stage, the formation of few filaments, and their coalescence into the single super-channel

https://doi.org/10.1017/S0022377899007515 Published online by Cambridge University Press

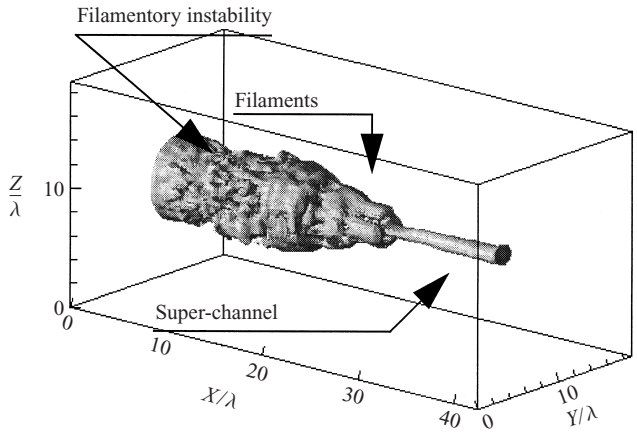


Figure 2. 3D perspective view of the self-focusing laser pulse, with $I_0 = 1.2 \times 10^{19}$ W cm^{-2} and radius $r = 6$ μm, in a plasma with $n = 0.36 n_c$.

due to the self-generated magnetic fields. The intensity in the super-channel rises from the initial $I_0 = 1.2 \times 10^{19}$ W cm^{-2} to 2×10^{20} W cm^{-2}, i.e. by a factor of about 18.

3. New features in the VLPL numerical scheme

A 2D geometry is discussed below for the sake of simplicity. Generalization to the 3D case used in VLPL is straightforward.

(i) *New Numerical Dispersion Free in the X direction (NDFX) scheme.* The space and time steps that one can use in a simulation have to be sufficiently small to 'resolve' the shortest wavelengths or the fastest oscillations of interest. Here one has to define the word 'resolve'. For linear waves, this means that a dispersion relation of a finite-difference (FD) approximation cannot significantly differ from the dispersion of initial continuum equations. For a standard FD approximation of the Maxwell equations. in vacuum on the Yee lattice in 2D planar geometry, one has a dispersion relation (Birdsall and Langdon 1991)

$$\frac{1}{c^2}\sin^2\frac{\omega\tau}{2} = \frac{\tau^2}{h_x^2}\sin^2\frac{k_x h_x}{2} + \frac{\tau^2}{h_y^2}\sin^2\frac{k_y h_y}{2}, \tag{3.1}$$

where h_x and h_y are the grid steps, τ is the time step, and ω, k_x and k_y are the frequency and the wave-vector components. For the limiting value of the time step $c^2\tau^2 = h_x^2 h_y^2/(h_x^2 + h_y^2)$ only the waves propagating along the grid diagonals are dispersion-free. This is seen in Fig. 3(a), where the numerical phase velocity $v_{\rm ph}/c = \omega/ck$ is shown. To send a laser along the grid diagonal is quite inconvenient from the programming point of view. Normally the laser propagates along one of the axes, and it is precisely here that the numerical dispersion is maximal. As a result, one has to use many cells per laser wavelength.

https://doi.org/10.1017/S0022377899007515 Published online by Cambridge University Press

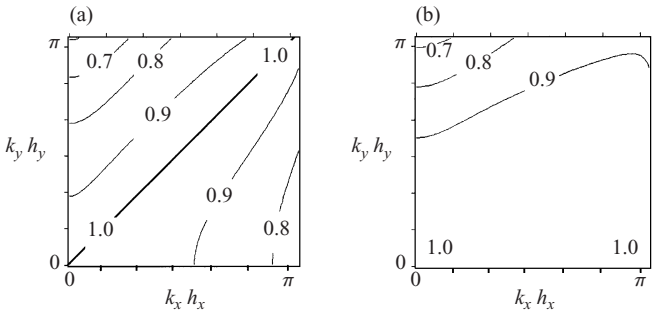


Figure 3. Numerical phase velocity $v_{\rm ph}/c$ corresponding (a) to the standard scheme (3.1) and (b) to the NDFX scheme (3.2) used in the VLPL code. The grid-cell aspect ratio $h_x/h_y = 0.5$. The scheme (3.1) is dispersionless along the mesh diagonals, $k_x = k_y$, while the NDFX scheme (3.2) is dispersionless for waves running in the X direction when $k_y = 0$.

The code VLPL uses another FD scheme. For the p polarization, this reads

$$\begin{aligned} B_{z\,i,j}^{\,n+1/2} - B_{z\,i,j}^{\,n-1/2} = {} & \frac{c\tau}{h_y}[\beta_x(E_{x\,i,j+1/2}^{\,n} - E_{x\,i,j-1/2}^{\,n}) \\ & +\alpha_x(E_{x\,i+1,j+1/2}^{\,n} - E_{x\,i+1,j-1/2}^{\,n} \\ & +E_{x\,i-1,j+1/2}^{\,n} - E_{x\,i-1,j-1/2}^{\,n})] \\ & -\frac{c\tau}{h_x}[\beta_y(E_{y\,i+1/2,j}^{\,n} - E_{y\,i-1/2,j}^{\,n}) \\ & +\alpha_y(E_{y\,i+1/2,j+1}^{\,n} - E_{y\,i-1/2,j+1}^{\,n} \\ & +E_{y\,i-1/2,j-1}^{\,n} - E_{y\,i-1/2,j-1}^{\,n})], \end{aligned} \tag{3.2a}$$

$$E_{x\,i,j+1/2}^{\,n+1} - E_{x\,i,j+1/2}^{\,n} = \frac{c\tau}{h_y}(B_{z\,i,j+1}^{\,n+1/2} - B_{z\,i,j}^{\,n+1/2}), \tag{3.2b}$$

$$E_{y\,i+1/2,j}^{\,n+1} - E_{y\,i+1/2,j}^{\,n} = \frac{c\tau}{h_x}(B_{z\,i+1,j}^{\,n+1/2} - B_{z\,i,j}^{\,n+1/2}), \tag{3.2c}$$

where

$$\beta_x = 0.75, \qquad \beta_y = 1 - 0.25(h_x/h_y)^2, \qquad \alpha_i = 0.5(1 - \beta_i),$$

and it is supposed that $h_x \leqslant h_y$. The dispersion relation for the NDFX scheme is

$$\frac{1}{\tau^2}\sin^2\frac{\omega\tau}{2} = \frac{1}{h_x^2}\sin^2\frac{k_x h_x}{2}(\beta_y + 2\alpha_y\cos k_y h_y) + \frac{1}{h_y^2}\sin^2\frac{k_y h_y}{2}(\beta_x + 2\alpha_x\cos k_x h_x). \tag{3.3}$$

As (3.3) shows, NDFX is stable even at $c\tau = h_x$. This is a unique property for an explicit multidimensional FD scheme. Using the NDFX scheme at this limit removes numerical dispersion for waves running along the X axis (the laser propagation direction) (see Fig. 3b), and for this reason the scheme is called NDFX: Numerical Dispersion Free in the X direction.

(ii) *Energy conservation.* The particles are cubes of constant charge density equal in size to the grid cells. The code VLPL uses an 'energy-conservative' (EC) algorithm of Villasenor and Buneman (1992) and Eastwood (1991). The field interpolation to particle positions for EC schemes is given in Hockney and Eastwood (1981). The present author has established experimentally that this scheme leads to the lowest numerical noise. Figure 4 shows the total energy evolution in an isolated system of

https://doi.org/10.1017/S0022377899007515 Published online by Cambridge University Press

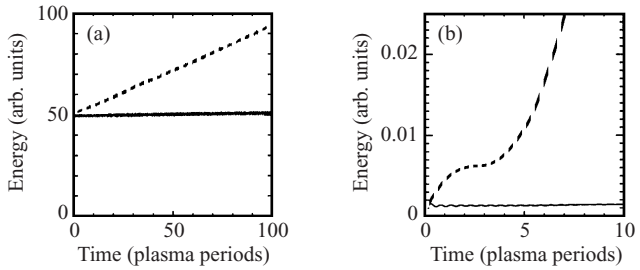


Figure 4. Energy conservation in the VLPL code due to the EC algorithm (solid lines) and numerical heating in the standard MC algorithm (dashed lines) when (a) the Debye length $D = 0.5h$, warm plasma, and (b) $D = 5 \times 10^{-3}h$, cold plasma. The energy change in the VLPL code is within 2% after 100 plasma periods.

particles for energy-conservative (solid lines) and a 'momentum-conservative' (MC) (Birdsall and Langdon 1991) (dashed lines) algorithms for two cases: (a) Debye length $D = 0.5h$ and (b) $D = 5 \times 10^{-3}h$. Although the energy conservation for the EC algorithm is not exact, it is much better than for the MC case. The actual energy change is only 2% over 100 plasma oscillations for the EC algorithm. This property makes it possible to simulate a cold plasma.

(iii) *Magnetic field interpolation.* One of the problems of PIC codes using the Yee lattice is that electric and magnetic fields are defined at different locations. This results in amplitude and phase errors when interpolated to the particle position. The standard approach (Birdsall and Langdon 1991) is to interpolate B fields to the cell vertices, first along the X direction,

$$B_{i+1/2,j} = 0.5(B_{i,j} + B_{i+1,j}), \tag{3.4}$$

and then along the Y direction. Making a Fourier analysis of (3.4), we find a dispersion relation connecting amplitudes of the wave originally existing on the mesh B_j^{orig} and of the interpolated harmonic B_j^{int}:

$$B_j^{\mathrm{int}} = B_j^{\mathrm{orig}} \cos \frac{k_x h_x}{2}. \tag{3.5}$$

From the dispersion relation (3.5), we see that the actual amplitude of the interpolated B field is significantly reduced for short wavelengths. The code VLPL uses a better four-point interpolation:

$$B_{i+1/2,j} = a(B_{i,j} + B_{i+1,j}) + b(B_{i-1,j} + B_{i+2,j}), \tag{3.6}$$

where $a + b = 0.5$. The dispersion relation for (3.6) is

$$B_j^{\mathrm{int}} = B_j^{\mathrm{orig}} \left(a \cos \frac{k_x h_x}{2} + b \cos \frac{3k_x h_x}{2} \right). \tag{3.7}$$

We have here a free paramter b, and may optimize the dispersion relation (3.7) by minimizing the integral of a square of deviation from the analytical solution:

$$\min_b \int_0^{k_{\max}} (B_j^{\mathrm{int}} - B_j^{\mathrm{orig}})^2 \, dk_x, \tag{3.8}$$

where $k_{\max}$ corresponds to the shortest wavelength in which we are still interested. Taking this shortest wavelength to be five mesh cells, i.e. $k_{\max} = 0.2\,\pi/h_x$, we find

https://doi.org/10.1017/S0022377899007515 Published online by Cambridge University Press

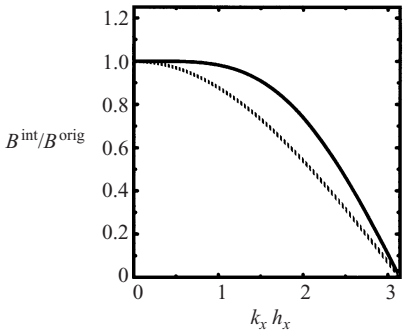


Figure 5. Ratio of the interpolated magnetic field B^{int} to the original B^{orig} as a function of the normalized wavenumber $k_x h_x$. The dotted line is for the standard interpolation (3.4); the solid line is for the optimized interpolation (3.6).

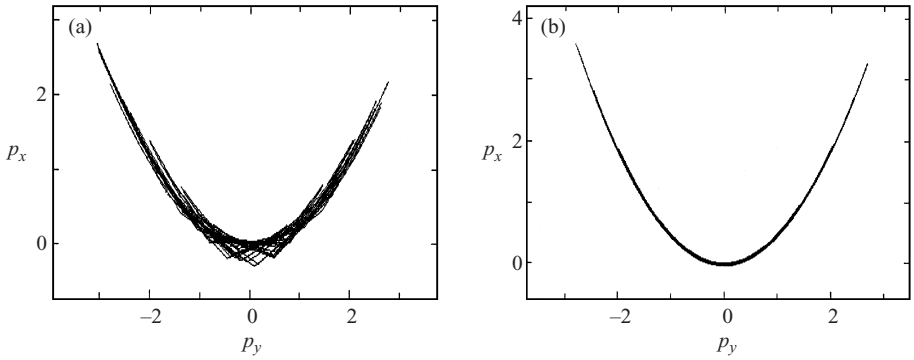


Figure 6. Figure-of-eight motion of a free electron in a plane electromagnetic wave with amplitude $a_0 = 3$. The analytical solution is $p_y = a(t)$; $p_x = \frac{1}{2}p_y^2$. The numerical result (a) corresponds to the standard B-field interpolation (3.4) for 10 grid cells per wavelength. The result (b) corresponds to the improved interpolation (3.6) used in VLPL; here we have only 8 cells per λ.

that the optimal parameters a and b are $a = 0.565$ and $b = -0.065$. The optimized interpolation (3.6) is of the same second-order accuracy as (3.5), but has a much flatter dispersion relation for $k < k_{\max}$, as seen in Fig. 5. Thus it does not disturb the B-field amplitude even for waves with wavelengths as short as five cells. This advantageous property is particularly important for a high-quality resolution of the figure-of-eight motion of an electron in a plane electromagnetic wave. Figure 6 shows numerical $p_\parallel$ ($p_\perp$) for a free electron in a plane electromagnetic wave with (a) interpolation like (3.4) with 10 cells per λ and (b) interpolation like (3.6) with only 8 cells per λ. The advantage of the scheme (3.6) is evident.

The above-mentioned improvements allow one to obtain high-quality results even with 8–10 cells per wavelength, and only a few (4–8) particles per cell (Borghesi et al. 1997; Pukhov and Meyer-ter-Vehn 1996, 1998).

3.1. Parallelization

The code VLPL uses a message passing interface for MPP communications. The algorithm is essentially local; thus only neighbouring processors need to communicate. This gives a very good linear scaling in the performance with the number of

https://doi.org/10.1017/S0022377899007515 Published online by Cambridge University Press

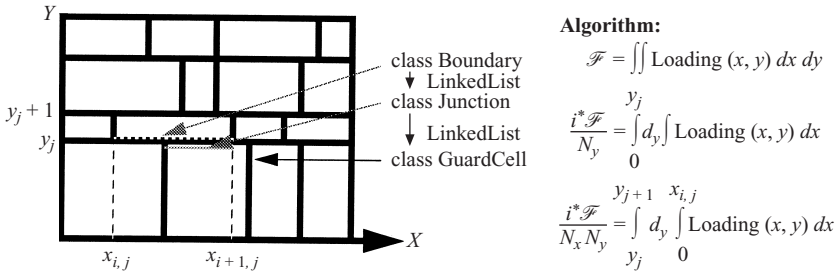


Figure 7. Load balancing in VLPL by adaptive partitioning: the example of a 2D 4 × 4 partitioning.

processing elements (PEs). The local algorithm and the object-oriented programming (OOP) technology allow for an adaptive partitioning to achieve a perfect load balancing among the processing elements. An example of the 2D domain partitioning is shown in Fig. 7. The interprocessor communications are handled by the class Junction which contains GuardCells as a linked list. Each GuardCell handles the particular data packing. Each Junction corresponds to an overlap of the neighbouring processors. The Boundary of each processor can have overlaps with several neighbours; thus it manages a linked list of the corresponding Junctions. OOP appears to be extremely useful for implementation of this.

3.2. Single-processor optimization

The new object-oriented C++ version of VLPL runs at more than 100 MFLOP per precessor on a Cray T3E-600 (3 μs per particle on a single PE). This is possible because of the special code structure. The particles are objects organized in linked lists with roots in the corresponding cells. Thus the code knows in advance which particles belong to which cell, and the loop that processes particles actually follows through the cells. The field information for the particular cell is stored into the cache, and then is used to process all the particles residing in this cell. This code structure effectively removes the cache trashing usual in other PIC codes with the standard organization of particles in a separate array, and one has to memory-sort particles from time to time (Decyk et al. 1996).

4. Conclusions

The three-dimensional particle-in-cell code VLPL (Virtual Laser Plasma Lab) allows for the first time direct 3D simulations of relativistic laser–plasma interactions starting from the most fundamental plasma model. This is possible due to

(i) improvements in the numerical scheme, which gives high-quality results even on coarse meshes with large time steps;

(ii) the use of massively parallel processing with more than 90% parallel efficiency and linear performance scaling with the number of processors;

(iii) aggressive single-processor optimization of the code.

Using 3D PIC simulations, we have studied relativistic laser self-focusing in a slightly underdense plasma, and have shown that background plasma electrons are accelerated to multi-MeV energies, producing strong currents and generating

https://doi.org/10.1017/S0022377899007515 Published online by Cambridge University Press

10^4 T magnetic fields. This physics is very important for the fast ignitor concept in inertial confinement fusion.

Acknowledgements

This work was supported by EURATOM, Deutsche Forschungsgemeinschaft, and Bundesmunisterium für Bildung und Forschung, Bonn.

References

Akhieser, A. I. and Polovin, R. V. 1956 *Soviet Phys. JETP* **3**, 696.

Askar'yan, G. A., Bulanov, S. V., Pegoraro, F. and Pukhov, A. M. 1994 *JETP Lett.* **60**, 251.

Birdsall, C. K. and Langdon, A. B. 1991 *Plasma Physics via Computer Simulations*. Adam Hilger, Bristol.

Borghesi, M., MacKinnon, A. J., Barringer, L., Gaillard, R., Gizzi, L. A., Meyer, C., Willi, O., Pukhov, A. and Meyer-ter-Vehn, J. 1997 *Phys. Rev. Lett.* **78**, 879.

Borisov, A. B., Borovskiy, A. V., Shiryaev, O. B., Korobkin, V. V., Prokhorov, A. M., Solem, J. C. et al. 1992 *Phys. Rev.* **A45**, 5830.

Bulanov, S. V., Pegoraro, F. and Pukhov, A. 1995 *Phys. Rev. Lett.* **74**, 710.

Bulanov, S. V., Pegoraro, F., Pukhov, A. and Sakharov, A. S. 1997 *Phys. Rev. Lett.* **78**, 4205.

Dawson, J. 1995 *Phys. Plasmas* **2**, 2189.

Decyk, V., Karmesin, S. R., de Boer, A. and Liewer, P. C. 1996 *Computers in Physics* **10**, 290.

Eastwood, J. 1991 *Comput. Phys. Commun.* **64**, 252.

Esarey, E., Krall, J. and Sprangle, Ph. 1994 *Phys. Rev. Lett.* **72**, 2887.

Esarey, E., Sprangle, P., Krall, J. and Ting, A. 1996 *IEEE Trans. Plasma Sci.* **24**, 252.

Fedoseevs, R., Wang, X. F. and Tsakiris, G. D. 1997 *Phys. Rev.* **E56**, 4615.

Hockney, R. W. and Eastwood, J. W. 1981 *Computer Simulation Using Particles*. McGraw-Hill, London.

Key, M. H., Cable, M. D., Cowan, T. E., Estabrook, K. G., Hammel, B. A., Hatchett, S. P. et al. 1998 *Phys. Plasmas* **5**, 1966.

Modena, A., Najmudin, Z., Dangor, A. E., Clayton, C. E., Marsh, K. A., Joshi, C. et al. 1995 *Nature* **377**, 606.

Mourou, G., Barty, C. and Perry, M. D. 1998 *Physics Today*, January, 22.

Pukhov A. and Meyer-ter-Vehn, J. 1996 *Phys. Rev. Lett.* **76**, 3975.

Pukhov, A. and Meyer-ter-Vehn, J. 1997 *Phys. Rev. Lett.* **79**, 2686.

Pukhov, A. and Meyer-ter-Vehn, J. 1998 *Phys. Plasmas* **5**, 1880.

Shvets, G. and Wurtele, J. 1994 *Phys. Rev. Lett.* **73**, 3540.

Tabak, M., Hammer, J., Glinsky, M. E., Kruer, W. L., Wilks, S. C., Woodworth, J., Campbell, E. M., Perry, M. D. and Mason, R. J. 1994 *Phys. Plasmas* **1**, 1626.

Umstadter, D., Chen, S.-Y., Maximchuk, A., Mourou, G. and Wagner, R. 1996 *Science* **273**, 472.

Villasenor, J. and Buneman, O. 1992 *Comput. Phys. Commun.* **69**, 306.

Wagner, R., Chen, S.-Y., Maksimchuk, A. and Umstadter, D. 1997 *Phys. Rev. Lett.* **78**, 3125.

https://doi.org/10.1017/S0022377899007515 Published online by Cambridge University Press